Real-Time Ground Fault Detection for Inverter-Based Microgrid Systems

JINGWEI DONG, YUCHENG LIAO, AND PEYMAN MOHAJERIN ESFAHANI

Abstract. Ground fault detection in inverter-based microgrid systems is challenging, particularly in a real-time setting, as the fault current deviates slightly from the nominal value. This difficulty is reinforced when natural disturbances exhibit similar output patterns as a faulty setting does. The conventional solution of installing more relays to obtain additional measurements is costly and also increases the complexity of the system. In this paper, we propose diagnosis schemes based on optimization-based fault detection filters with the output current as the only measurement. Modeling the microgrid dynamics and the diagnosis filter, we formulate the filter design as a linear programming (LP) problem that accounts for decoupling a class of disturbances and ensuring fault sensitivity simultaneously. Next, we robustify the filter to disturbances that cannot be fully decoupled. To this end, we leverage tools from the existing literature and extend the optimization program to a quadratic programming (QP) problem in which the filter is trained for this class of disturbances. To ease the computational effort, we also provide an approximate but analytical solution to this QP. Additionally, we use classical statistical results to provide a thresholding mechanism that enjoys probabilistic false-alarm guarantees. Finally, we verify the effectiveness of the proposed methods through several numerical simulations.

1. Introduction

In the past decade, inverter-based microgrid systems have gained popularity as power systems become increasingly complex and rely more on renewable energy sources [1]. These microgrid systems help integrate renewable energy sources into power systems and regulate the amount of power supplied to customers to provide high-quality power and reduce energy costs. They can also operate independently and allow for local control of distributed generation, for example, when the main grid is unavailable due to blackouts or storms [2]. This greatly increases the reliability of power systems.

Although inverter-based microgrid systems offer many benefits, they are susceptible to faults that can pose safety risks and damage equipment. Therefore, it is crucial to promptly and accurately detect faults to ensure the safe operation of inverter-based microgrid systems. However, the conventional protection strategy for power systems, such as overcurrent detection, is inefficient in detecting faults in inverter-based microgrid systems [3]. This is because the fault current only slightly deviates from the nominal value due to a current limiter embedded in the inverter controller [4]. According to IEEE Std. 1547.2 [5], the inverter current when the microgrid systems work in the islanded mode is restricted to 1-2 times the rated current during short-circuit faults. The fault detection problem

Date: May 12, 2023.

The authors are with the Delft Center for Systems and Control, Delft University of Technology, The Netherlands ({J.Dong-6, P.MohajerinEsfahani}@tudelft.nl, Y.Liao-3@student.tudelft.nl). This work is supported by the ERC (European Research Council) grant TRUST-949796 and CSC (China Scholarship Council) with funding number: 201806120015.

is more difficult when considering disturbances that have similar effects on the output current as faults. Therefore, developing an effective fault detection scheme for inverter-based microgrid systems in the presence of disturbances remains a challenge, particularly when the output current is the only measurement. In this paper, we focus on the detection of ground faults as they are the most common and problematic type of faults in inverter-based microgrid systems [6].

To address the fault detection problem for microgrid systems, researchers have developed several differential methods that rely on communication infrastructures between relays. These methods measure the difference in the current symmetrical components [7], the energy content of current [8], the instantaneous current with comparative voltage [9], and the traveling wave polarities [10, 11] to detect faults. Though these methods have shown effectiveness, relying on communication devices can reduce the reliability of systems as they are vulnerable to faults and cyber attacks. Moreover, most differential methods require the installation of new equipment, such as relays and communication infrastructure, which can be expensive and time-consuming to implement and maintain.

In addition to differential methods, active fault detection methods have emerged as another popular solution to fault detection for microgrid systems in recent years. By introducing carefully designed input signals into the system, active fault detection methods can enhance the detectability of faults. In [12], the authors inject a small negative-sequence current ($< 3\%$) into the microgrid system and detect faults by using a signal processing technique to quantify the resulting negative-sequence voltage. Most recently, the authors in [13] provide an optimal input design method ensuring that the output sets of normal and faulty modes of an inverter-based microgrid system are separated with a probabilistic guarantee. Then, it compares the output of the real-time process with the output sets to generate diagnosis results. However, the injected input signals can degrade the system performance to some extent. Additionally, to obtain optimal input sequences as described in [13], an optimization problem must be solved each time, which can be computationally intensive and is unsuitable for online monitoring.

In contrast to differential methods, fault detection methods based on residual generation can be less dependent on the communication infrastructure and additional sensors, as these methods make full use of modeling information of systems. Moreover, residual generation-based methods are more suitable for online monitoring than active fault detection methods since they do not require continuous updates and have no impact on system performance. Let us briefly review several approaches to designing a residual generator. In the field of fault detection, the residual generator is generally constructed using observer-based or parity-space methods [14]. To handle disturbances, optimization techniques can be employed to determine the parameters of the residual generator, ensuring that the residual is sensitive to faults while being robust against disturbances [15, 16]. Alternatively, decomposition techniques such as the unknown input observer (UIO) [17] can be utilized to decouple disturbances from the residual. However, we found that the UIO approach could fail to satisfy the detectability condition when applied to inverter-based microgrid systems with a limited number of measurements, even when disturbances can be fully decoupled. In [18], the authors propose a parity-space-like approach for designing residual generators in the framework of the linear differential-algebraic equation (DAE). The derived residual generator can have lower order than that of the system, which reduces computational complexity when dealing with large-scale systems. Additionally, this framework provides design freedom. In specific, one is able to transform the design of the residual generator into various optimization problems to obtain desired solutions based on different requirements, such as disturbance decoupling [18], nonlinear suppression [19], and model mismatch handling [20] in fault detection tasks, as well as multiple fault estimation [21].

Main contributions: In this work, we leverage the advantages of the DAE framework to design fault detection filters for inverter-based microgrid systems. To the best of our knowledge, this is the first attempt to design fault detection filters using the DAE framework that enables real-time monitoring of ground faults in inverter-based microgrid systems. It is worth noting that disturbances may not be completely decoupled in some scenarios because of the limited number of sensors in the systems. The contributions of this paper are summarized as follows:

- **Dynamic system modeling:** We develop a unified state-space model for the inverter-based microgrid system in both normal mode and the presence of ground faults (Sections 2.2, 2.3). This model is further formulated in the DAE framework, which facilitates the design of robust fault detection filters.
- **Linear programming design for perfect setting:** We formulate the design of fault detection filters into a LP problem (Proposition 3.1), which achieves disturbance decoupling and ensures fault sensitivity simultaneously.
- **Data-assisted disturbance rejection:** To deal with non-decoupled disturbances, we borrow ideas from [19, Approach (II)] to extend the design to a QP problem, wherein the average effects of available disturbance patterns on the residual are minimized (Theorem 3.3). Inspiring from [22, Corollary 1], we also obtain an approximate analytical solution to this QP problem with arbitrary accuracy (Corollary 3.4), allowing for online updates of filter parameters.
- **Probabilistic false alarm certificate:** Leveraging the classical Markov inequality, we further propose a threshold determination method along with probabilistic false-alarm guarantees (Proposition 3.8).

The rest of the paper is organized as follows. The modeling of an inverter-based microgrid system and the problem formulation are presented in Section 2. In Section 3, we provide design methods for the fault detection filters. In Section 4, we evaluate the effectiveness of the proposed approaches with numerical simulations. Finally, Section 5 concludes the paper with some remarks and future directions.

Notation: Sets $\mathbb{R}(\mathbb{R}_+)$ and $\mathbb{N}$ denote all (positive) reals and non-negative integers, respectively. The space of n dimensional real-valued vectors is denoted by $\mathbb{R}^n$. For a vector $v = [v_1, \ldots, v_n]$, the infinity-norm of v is $\|v\|_\infty = \max_{i\in\{1,\ldots,n\}} |v_i|$. The operator $\mathrm{diag}(v)$ constructs a diagonal matrix from the vector v. For two discrete-time signals σ_1 and σ_2 taking values in $\mathbb{R}^n$ with length T, the $\mathcal{L}_2$ inner product is represented as $\langle \sigma_1, \sigma_2 \rangle := \sum_{k=1}^{T} \sigma_1^\top(k)\sigma_2(k)$, and the corresponding norm $\|\sigma_1\|_{\mathcal{L}_2} := \sqrt{\langle \sigma_1, \sigma_1 \rangle}$. The notation $\mathbf{0}_{m\times n}$ denotes a zero matrix with m rows and n columns. The identity matrix with an appropriate dimension is denoted by I. For a random variable χ, $\mathbf{Pr}[\chi]$ and $\mathbf{E}[\chi]$ are the probability law and the expectation of χ.

2. Modeling and Problem Statement

In this section, we present the state-space model of an inverter-based microgrid system and consider three-phase symmetrical ground faults. Then, we formulate the two problems addressed in this work.

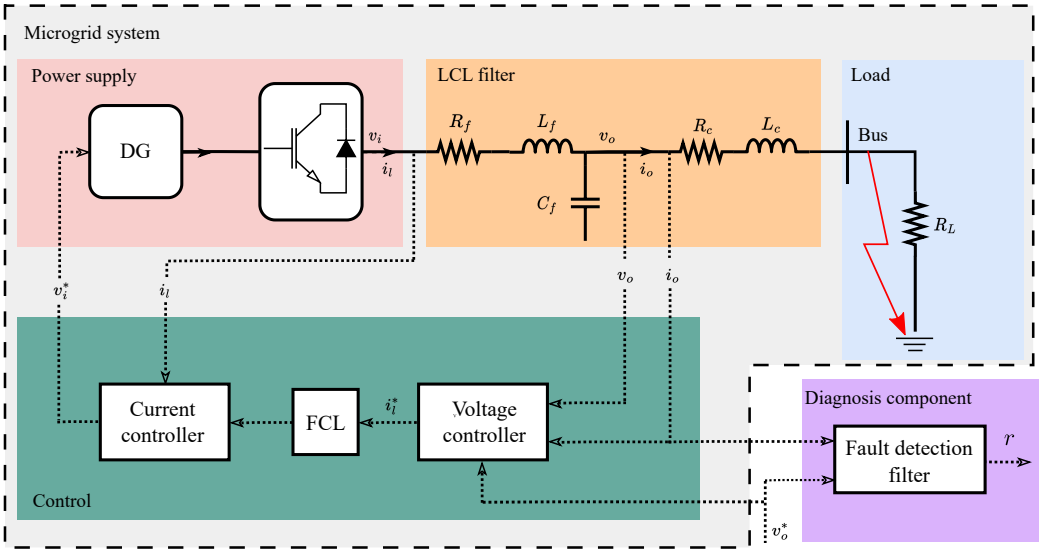

FIGURE 1. Architecture of an inverter-based microgrid system with the diagnosis component.

2.1. System description

An inverter-based microgrid generally consists of four components: the power supplier, the LCL filter, the controller, and the load, as shown in Figure 1. Let us elaborate on the functions of each component.

(1) **Power supplier**: The power supply part provides power to the microgrid by following a reference voltage v_i^* from the current controller. It contains a distributed generator (DG) source and an inverter. In this work, we make two assumptions: (1) an ideal DG source is available, and (2) the inverter switching process can be neglected due to its high switching frequency. Therefore, instead of modeling the generator and inverter, we can set the output voltage of the inverter directly to $v_i = v_i^*$. The real-time output current of the inverter is denoted by i_l. As the single DG source supplies all power to the load, droop control is unnecessary, and the microgrid frequency ω is constant. This differs from [23], where multiple DG sources operate simultaneously.

(2) **LCL filter**: The LCL filter is used to filter the harmonics produced by the inverter. It consists of two resistors R_f and R_c, two inductors L_f and L_c, and a capacitor C_f. The signals v_o and i_o denote the grid-side voltage and the output current, respectively.

(3) **Controller**: The control part keeps the grid-side voltage at some reference voltage $v_o^*(t)$. This can be achieved through an inner current controller and an outer voltage controller, which are all PI controllers [24]. The outer voltage controller sets reference $i_l^*(t)$ for the inner current controller. The fault current limiter (FCL) is a saturation block that protects the microgrid from large fault currents.

(4) **Load**: We assume the load denoted by R_L is purely resistive. Note that the unknown part of the load is the main source of disturbances.

The mentioned voltage and current are based on a three-phase system. We introduce the direct-quadrature (dq) transform to simplify the analysis. Specifically, for a three-phase system with current $i = [i_a\ i_b\ i_c]^\top$ and voltage $v = [v_a\ v_b\ v_c]^\top$ in the abc framework, the dq transform projects $i(t)$

and $v(t)$ onto dq-axis, i.e., $i_{dq} = \mathbf{P}i,\ v_{dq} = \mathbf{P}v$, where $i_{dq} = [i_d\ i_q]^\top,\ v_{dq} = [v_d\ v_q]^\top$. The projection matrix $\mathbf{P}$ is given by

$$\mathbf{P} = \frac{2}{3}\begin{bmatrix} \cos(\theta) & \cos\left(\theta - \frac{2\pi}{3}\right) & \cos\left(\theta + \frac{2\pi}{3}\right) \\ \sin(\theta) & \sin\left(\theta - \frac{2\pi}{3}\right) & \sin\left(\theta + \frac{2\pi}{3}\right) \end{bmatrix},$$

in which θ is the constantly changing angle between the d-axis and the a-axis. We refer interested readers to [25] for more details about the dq transformation. For simplicity of expression, we add subscripts to indicate the variables after dq transformation throughout the paper, e.g., $v \xrightarrow{dq} v_{dq}$, $i \xrightarrow{dq} i_{dq}$, and so forth.

2.2. State-space model of the fault-free microgrid system

To obtain the state-space model of the fault-free microgrid system, we first model individual components of the microgrid including the voltage controller, the current controller, and the LCL filter in this subsection.

We start with the voltage controller in the control component. Let us transform v_o, v_o^*, i_o and i_l^* into the dq framework, which are v_{odq}, v_{odq}^*, i_{odq} and i_{ldq}^*, respectively. We further define the cumulative error between v_{odq} and v_{odq}^* by $\phi_{dq} := [\phi_d\ \phi_q]^\top$, which can be written as

$$\frac{\mathrm{d}\phi_d(t)}{\mathrm{d}t} = v_{od}^*(t) - v_{od}(t), \quad \frac{\mathrm{d}\phi_q(t)}{\mathrm{d}t} = v_{oq}^*(t) - v_{oq}(t). \tag{1}$$

Considering that the voltage controller is a PI controller, based on Kirchhoff's laws, we obtain

$$\begin{cases} i_{ld}^*(t) = Fi_{od}(t) - \omega C_f v_{oq}(t) + K_P^v\left(v_{od}^*(t) - v_{od}(t)\right) + K_I^v\phi_d(t), \\ i_{lq}^*(t) = Fi_{oq}(t) + \omega C_f v_{od}(t) + K_P^v\left(v_{oq}^*(t) - v_{oq}(t)\right) + K_I^v\phi_q(t), \end{cases} \tag{2}$$

where F is the feedforward coefficient, K_P^v and K_I^v denote the proportional and integral gains of the voltage controller, respectively. From (1) and (2), we obtain the state-space model of the voltage controller

$$\begin{cases} \dot{\phi}_{dq}(t) = B_{v1}v_{odq}^*(t) + B_{v2}\left[i_{ldq}(t) \quad v_{odq}(t) \quad i_{odq}(t)\right]^\top, \\ i_{ldq}^*(t) = C_v\phi_{dq}(t) + D_{v1}v_{odq}^*(t) + D_{v2}\left[i_{ldq}(t) \quad v_{odq}(t) \quad i_{odq}(t)\right]^\top, \end{cases} \tag{3}$$

where the matrices are

$$B_{v1} = \begin{bmatrix} 1 & 0 \\ 0 & 1 \end{bmatrix},\ B_{v2} = \begin{bmatrix} 0 & 0 & -1 & 0 & 0 & 0 \\ 0 & 0 & 0 & -1 & 0 & 0 \end{bmatrix},\ C_v = \begin{bmatrix} K_I^v & 0 \\ 0 & K_I^v \end{bmatrix},$$

$$D_{v1} = \begin{bmatrix} K_P^v & 0 \\ 0 & K_P^v \end{bmatrix},\ D_{v2} = \begin{bmatrix} 0 & 0 & -K_P^v & -\omega C_f & F & 0 \\ 0 & 0 & \omega C_f & -K_P^v & 0 & F \end{bmatrix}.$$

Similarly, one can obtain the state-space model of the current controller. Let us transform i_l, i_l^* and v_i^* into the dp framework, which are i_{ldq}, i_{ldq}^* and v_{idq}^*, respectively. The cumulative error between i_{ldq} and i_{ldq}^* is denoted by $\gamma_{dq} := [\gamma_d\ \gamma_q]^\top$, i.e.,

$$\frac{\mathrm{d}\gamma_d(t)}{\mathrm{d}t} = i_{ld}^*(t) - i_{ld}(t), \quad \frac{\mathrm{d}\gamma_q(t)}{\mathrm{d}t} = i_{lq}^*(t) - i_{lq}(t). \tag{4}$$

Then, the dynamics of the current controller follows

$$\begin{cases} v_{id}^*(t) = -\omega L_f i_{lq}(t) + K_P^c\left(i_{ld}^*(t) - i_{ld}(t)\right) + K_I^c\gamma_d(t), \\ v_{iq}^*(t) = \omega L_f i_{ld}(t) + K_P^c(i_{lq}^*(t) - i_{lq}(t)) + K_I^c\gamma_q(t), \end{cases} \tag{5}$$

where K_P^c and K_I^c denote the proportional and integral gains of the current controller, respectively. Based on (4) and (5), the state-space model of the current controller is given by

$$\begin{cases} \dot{\gamma}_{dq}(t) = B_{c1} i^*_{ldq}(t) + B_{c2} \begin{bmatrix} i_{ldq}(t) & v_{odq}(t) & i_{odq}(t) \end{bmatrix}^\top, \\ v^*_{idq}(t) = C_c \gamma_{dq}(t) + D_{c1} i^*_{ldq}(t) + D_{c2} \begin{bmatrix} i_{ldq}(t) & v_{odq}(t) & i_{odq}(t) \end{bmatrix}^\top, \end{cases} \tag{6}$$

where

$$B_{c1} = \begin{bmatrix} 1 & 0 \\ 0 & 1 \end{bmatrix},\ B_{c2} = \begin{bmatrix} -1 & 0 & \mathbf{0}_{1\times 4} \\ 0 & -1 & \mathbf{0}_{1\times 4} \end{bmatrix},\ C_c = \begin{bmatrix} K_I^c & 0 \\ 0 & K_I^c \end{bmatrix},$$
$$D_{c1} = \begin{bmatrix} K_P^c & 0 \\ 0 & K_P^c \end{bmatrix},\ D_{c2} = \begin{bmatrix} -K_P^c & -\omega L_f & \mathbf{0}_{1\times 4} \\ \omega L_f & -K_P^c & \mathbf{0}_{1\times 4} \end{bmatrix}.$$

For the LCL filter modeling, we transform the output voltage of the inverter v_i and the bus voltage v_b into the dq framework, i.e., v_{idq} and v_{bdq}, respectively. By applying Kirchhoff's laws, we get the dynamics of the LCL filter as follows

$$\begin{cases} \dot{i}_{ld}(t) = \frac{-R_f}{L_f} i_{ld}(t) + \omega i_{lq}(t) + \frac{1}{L_f} v_{id}(t) - \frac{1}{L_f} v_{od}(t), \\ \dot{i}_{lq}(t) = \frac{-R_f}{L_f} i_{lq}(t) - \omega i_{ld}(t) + \frac{1}{L_f} v_{iq}(t) - \frac{1}{L_f} v_{oq}(t), \\ \dot{v}_{od}(t) = \omega v_{oq}(t) + \frac{1}{C_f} i_{ld}(t) - \frac{1}{C_f} i_{od}(t), \\ \dot{v}_{oq}(t) = -\omega v_{od}(t) + \frac{1}{C_f} i_{lq}(t) - \frac{1}{C_f} i_{oq}(t), \\ \dot{i}_{od}(t) = \frac{-R_c}{L_c} i_{od}(t) + \omega i_{oq}(t) + \frac{1}{L_c} v_{od}(t) - \frac{1}{L_c} v_{bd}(t), \\ \dot{i}_{oq}(t) = \frac{-R_c}{L_c} i_{oq}(t) - \omega i_{od}(t) + \frac{1}{L_c} v_{oq}(t) - \frac{1}{L_c} v_{bq}(t). \end{cases}$$

The state-space model of the LCL filter is

$$\begin{bmatrix} \dot{i}_{ldq}(t) \\ \dot{v}_{odq}(t) \\ \dot{i}_{odq}(t) \end{bmatrix} = A_l \begin{bmatrix} i_{ldq}(t) \\ v_{odq}(t) \\ i_{odq}(t) \end{bmatrix} + \begin{bmatrix} B_{l1} & B_{l2} \end{bmatrix} \begin{bmatrix} v_{idq}(t) \\ v_{bdq}(t) \end{bmatrix}, \tag{7}$$

where the bus voltage $v_{bdq}(t) = \begin{bmatrix} R_L & 0 \\ 0 & R_L \end{bmatrix} i_{odq}(t)$, and the matrices are

$$A_l = \begin{bmatrix} -\frac{R_f}{L_f} & \omega & -\frac{1}{L_f} & 0 & 0 & 0 \\ -\omega & -\frac{R_f}{L_f} & 0 & -\frac{1}{L_f} & 0 & 0 \\ \frac{1}{C_f} & 0 & 0 & \omega & -\frac{1}{C_f} & 0 \\ 0 & \frac{1}{C_f} & -\omega & 0 & 0 & -\frac{1}{C_f} \\ 0 & 0 & \frac{1}{L_c} & 0 & -\frac{R_c}{L_c} & \omega \\ 0 & 0 & 0 & \frac{1}{L_c} & -\omega & -\frac{R_c}{L_c} \end{bmatrix}, B_{l1} = \begin{bmatrix} \frac{1}{L_f} & 0 & \mathbf{0}_{1\times 4} \\ 0 & \frac{1}{L_f} & \mathbf{0}_{1\times 4} \end{bmatrix}^\top,\ B_{l2} = \begin{bmatrix} \mathbf{0}_{1\times 4} & -\frac{1}{L_c} & 0 \\ \mathbf{0}_{1\times 4} & 0 & -\frac{1}{L_c} \end{bmatrix}^\top.$$

Recall that $v_i = v_i^*$, and thus $v_{idq} = v^*_{idq}$. By combining the derived models (3), (6), and (7), we obtain the complete state-space model of the inverter-based microgrid system in the fault-free case

$$\begin{cases} \dot{x}(t) = A_h x(t) + B_h v^*_{odq}(t) + B_d d(t), \\ i_{odq}(t) = C x(t), \end{cases} \tag{8}$$

where $x(t) = \begin{bmatrix} \phi_{dq}^\top(t) & \gamma_{dq}^\top(t) & i_{ldq}^\top(t) & v_{odq}^\top(t) & i_{odq}^\top(t) \end{bmatrix}^\top$ is the augmented state of the microgrid system and $d(t)$ denotes the disturbance. The system matrices A_h, B_h, and C are given by

$$A_h = \begin{bmatrix} \mathbf{0}_{2\times 2} & \mathbf{0}_{2\times 2} & B_{v2} \\ B_{c1} C_v & \mathbf{0}_{2\times 2} & B_{c1} D_{v2} + B_{c2} \\ B_{l1} D_{c1} C_v & B_{l1} C_c & A_{h33} \end{bmatrix},\ B_h = \begin{bmatrix} B_{v1} \\ B_{c1} D_{v1} \\ B_{l1} D_{c1} D_{v1} \end{bmatrix},\ C = \begin{bmatrix} \mathbf{0}_{2\times 8} & I \end{bmatrix},$$

where $A_{h33} = A_l + B_{l1}\left(D_{c1}D_{v2} + D_{c2}\right) + B_{l2}\begin{bmatrix} R_L & 0 \\ 0 & R_L \end{bmatrix}\begin{bmatrix}\mathbf{0}_{2\times 4} & I\end{bmatrix}$. We would like to highlight that the number of states is 10, while we only have 2 measurements. Referring to [23, 26], we consider that changes in the load component can result in deviations from the nominal value of the output current i_{odq}. Furthermore, the following assumption on the matrix B_d is introduced to describe the impact of d on the system.

Assumption 2.1 (Disturbance description)**.** *The disturbance d directly influences the output current i_{odq}, which is characterized through the matrix B_d. In this work, we consider both one-dimensional and two-dimensional disturbances. The structure of B_d is: (1) $B_d = \begin{bmatrix}\mathbf{0}_{1\times 8} & [\xi_1\ \xi_2]\end{bmatrix}^\top$ for $d(t) \in \mathbb{R}$, and (2) $B_d = \begin{bmatrix}\mathbf{0}_{2\times 8} & \mathrm{diag}([\xi_1\ \xi_2])\end{bmatrix}^\top$ for $d(t) \in \mathbb{R}^2$, where $\xi_1, \xi_2 \in \mathbb{R}$ represent the level of disturbance in the corresponding channel.*

Remark 2.2 (Disturbance decoupling condition)**.** *Let $\mathbb{T}_{di_{odq}}$ denote the transfer function from the disturbance d to the measurement i_{odq}, and $Rank(\mathbb{T}_{di_{odq}})$ denotes the rank of $\mathbb{T}_{di_{odq}}$. According to [27, Chapter 6], d can be decoupled from i_{odq} if the number of unknown inputs is smaller than the number of sensors, i.e., $Rank(\mathbb{T}_{di_{odq}}) < 2$. Therefore, d can be decoupled from $i_{odq}(t)$ when $d(t)$ is a one-dimensional signal but not for a two-dimensional (and higher-dimensional) disturbance.*

2.3. State-space model of the microgrid system with ground faults

We consider three-phase symmetrical ground faults which can cause a short circuit and a sharp increase in the output current i_{odq}. Therefore, we know that after ground faults occur: (1) the load $R_L = 0$ because of the short circuit, leading to a zero bus voltage $v_{bdq} = 0$; and (2) the output of the voltage controller i^*_{ldq} saturates to a constant value τ_{dq} immediately, i.e., $i^*_{ldq}(t) = \tau_{dq}$ for $t \geq t_f$, where t_f denotes the time instant when the faults occur.

The state-space model of the current controller (6) in the fault scenario becomes

$$\begin{cases} \dot{\gamma}_{dq}(t) = B_{c1}\tau_{dq} + B_{c2}\begin{bmatrix} i_{ldq}(t) & v_{odq}(t) & i_{odq}(t)\end{bmatrix}^\top, \\ v^*_{idq}(t) = C_c\gamma_{dq}(t) + D_{c1}\tau_{dq} + D_{c2}\begin{bmatrix} i_{ldq}(t) & v_{odq}(t) & i_{odq}(t)\end{bmatrix}^\top. \end{cases} \tag{9}$$

Based on (3), (7), and (9), the state-space model of the inverter-based microgrid system with ground faults can be written as

$$\begin{cases} \dot{x}(t) = A_{uh}x(t) + B_{uh1}v^*_{odq}(t) + B_{uh2}\tau_{dq}, \\ i_{odq}(t) = Cx(t), \end{cases} \tag{10}$$

where the matrices A_f, B_{uh1}, and B_{uh2} are

$$A_{uh} = \begin{bmatrix} \mathbf{0}_{2\times 2} & \mathbf{0}_{2\times 2} & B_{v2} \\ \mathbf{0}_{2\times 2} & \mathbf{0}_{2\times 2} & B_{c2} \\ \mathbf{0}_{6\times 2} & B_{l1}C_c & A_l + B_{l1}D_{c2} \end{bmatrix},\ B_{uh1} = \begin{bmatrix} B_{v1} \\ \mathbf{0}_{2\times 2} \\ \mathbf{0}_{6\times 2} \end{bmatrix},\ B_{uh2} = \begin{bmatrix} \mathbf{0}_{2\times 2} \\ B_{c1} \\ B_{l1}D_{c1} \end{bmatrix}.$$

Note that the disturbance $d(t)$ has no effect on the system in the fault scenario because of the short circuit.

To write the normal and faulty models (8) and (10) into a more compact form, we introduce a signal $f(t)$ to indicate the occurrence of ground faults, i.e.,

$$\begin{cases} f(t) = 0, & \text{no faults}, \\ f(t) = 1, & \text{faults happen}. \end{cases}$$

With $f(t)$, we can express the normal and faulty models in the following unified form

$$\begin{cases} \dot{x}(t) = \mathcal{A}(f(t))x(t) + \mathcal{B}_u(f(t))u(t) + \mathcal{B}_d(f(t))d(t), \\ y(t) = Cx(t), \end{cases} \tag{11}$$

where $u(t) = [v^*_{odq}(t)\ \tau_{dq}]^\top$ consists of the known input signals, $y(t) = i_{odq}(t)$ is the output. The dimensions of $x(t),\ u(t),\ d(t)$ and $y(t)$ are denoted by $n_x,\ n_u,\ n_d$, and n_y, respectively. The system matrices are

$$\mathcal{A}(f(t)) = A_h + f(t)(A_{uh} - A_h),\ \mathcal{B}_u(f(t)) = [B_h + f(t)(B_{uh1} - B_h) \quad f(t)B_{uh2}],$$
$$\mathcal{B}_d(f(t)) = (1 - f(t))B_d.$$

Remark 2.3 (Discretization)**.** *Considering that the discrete-time samplings of data are used in the realistic framework, we discretize the continuous-time state-space model* (11) *when designing the fault diagnosis scheme. In what follows, all signals are presented in the discrete-time form. For convenience, we use the same notation for system matrices in both the continuous and discrete representations.*

2.4. **Problem statement**

The objective of this work is to detect the occurrence of ground faults in the presence of the disturbance d using the input u and the measurement y. Our proposed diagnosis scheme is to design a residual generator denoted by a linear transfer function $\mathbb{F}$, whose output is a scalar-valued signal $r := \mathbb{F}[y^\top\ u^\top]^\top$ (called the residual). The structure is illustrated in the diagnosis component of Fig. 1. The residual r should be sensitive to the fault mode and exhibit robustness to the disturbance. Ideally, in the absence of ground faults, the residual should remain close to zero. However, the residual can exhibit a significant increase to facilitate detection when ground faults occur. Then, two questions arise naturally. How can we design $\mathbb{F}$ to achieve the following goals:

(1) Suppress the contribution of the disturbance to the residual in the normal mode;
(2) Enhance the fault sensitivity of the residual in the faulty mode.

In this work, we provide a design method of the filter $\mathbb{F}$ in the DAE framework to satisfy the above two design requirements. To this end, let us introduce the shift operator $\mathfrak{q}$, i.e., $\mathfrak{q}x(k) = x(k+1)$, and transform the discrete-time version of the unified state-space model (11) into

$$H(\mathfrak{q}, f)[X] + L(\mathfrak{q}, f)[Y] = 0, \tag{12}$$

where $X = [x^\top\ d^\top]^\top$, $Y = [y^\top\ u^\top]^\top$. The matrices $H(\mathfrak{q}, f)$ and $L(\mathfrak{q}, f)$ are polynomial functions in the operator $\mathfrak{q}$, depending on the indicator signal $f \in \{0, 1\}$, which are

$$H(\mathfrak{q}, f) = \mathfrak{q}H_1 + H_0(f) = \begin{bmatrix} -\mathfrak{q}I + \mathcal{A}(f) & \mathcal{B}_d(f) \\ C & 0 \end{bmatrix},\ H_1 = \begin{bmatrix} -I & 0 \\ 0 & 0 \end{bmatrix},\ H_0(f) = \begin{bmatrix} \mathcal{A}(f) & \mathcal{B}_d(f) \\ C & 0 \end{bmatrix},$$
$$L(\mathfrak{q}, f) = \begin{bmatrix} 0 & \mathcal{B}_u(f) \\ -I & 0 \end{bmatrix}.$$

Since $L(\mathfrak{q}, f)$ is independent of $\mathfrak{q}$, we define $L(\mathfrak{q}, 0) = L_0$ and $L(\mathfrak{q}, 1) = L_1$.

The fault detection filter $\mathbb{F}$ is in the form of

$$\mathbb{F}(\mathfrak{q}) = \frac{1}{a(\mathfrak{q})} N(\mathfrak{q}) L_0, \tag{13}$$

where the numerator $N(\mathfrak{q})$ is a polynomial row vector $N(\mathfrak{q}) = \sum_{i=0}^{d_N} N_i \mathfrak{q}^i$, $N_i \in \mathbb{R}^{1\times(n_x+n_y)}$, d_N is the degree of $N(\mathfrak{q})$. The denominator $a(\mathfrak{q})$ is a polynomial with a degree larger than d_N and all roots inside the unit circle so that the derived filter is strictly proper and stable. For simplicity of design, we fix d_N and $a(\mathfrak{q})$ and only design the coefficients of $N(\mathfrak{q})$. It is worth pointing out that $a(\mathfrak{q})$ can be chosen up to the user and specific requirements, e.g., noise sensitivity and dynamic performance, which will be our future research.

By setting $f = 0$ and multiplying from the left-hand side of (12) by $a^{-1}(\mathfrak{q})N(\mathfrak{q})$, we obtain the residual r in the normal mode, which is

$$r = \frac{1}{a(\mathfrak{q})}N(\mathfrak{q})L_0[Y] = -\frac{1}{a(\mathfrak{q})}N(\mathfrak{q})H(\mathfrak{q},0)[X]. \tag{14}$$

When ground faults happen, i.e., $f = 1$, DAE model (12) becomes $H(q,1)[X]+L_1[Y] = 0$. Thus, $Y = -L_1^{\dagger}H(q,1)[X]$, where $L_1^{\dagger}$ is the left inverse of L_1. The residual r in the fault mode becomes

$$r = \frac{1}{a(\mathfrak{q})}N(\mathfrak{q})L_0[Y] = -\frac{1}{a(\mathfrak{q})}N(\mathfrak{q})L_0L_1^{\dagger}H(q,1)[X]. \tag{15}$$

Note that all the entities in $a^{-1}(\mathfrak{q})N(\mathfrak{q})L_0[Y]$ are known and thus can be used to generate the residual. The right-hand side of (14) and (15) characterize the mapping relations between the unknown signal X and r in the normal and faulty modes, respectively, based on which we can design $\mathbb{F}(\mathfrak{q})$ for different diagnosis purposes.

First, we consider the one-dimensional disturbance that can be fully decoupled. To ensure that the residual is zero in the normal mode and sensitive to the faulty mode, i.e., $r = 0$ when $f = 0$ and $r \neq 0$ when $f = 1$, we introduce the following conditions:

$$N(\mathfrak{q})H(\mathfrak{q},0) = 0, \tag{16a}$$

$$N(\mathfrak{q})L_0L_1^{\dagger}H(q,1) \neq 0. \tag{16b}$$

In view of the desired mapping relations (16a) and (16b), we proceed with the first problem.

Problem 1. (Fault detection filter design for perfect setting) *Consider the state-space model of the inverter-based microgrid system* (11) *with three-phase symmetrical ground faults and Assumption 2.1 with* $n_d = 1$. *Design a fault detection filter* $\mathbb{F}$ *in the form of* (13) *that satisfies* (16a) *and* (16b).

Remark 2.4 (Existence of $L_1^{\dagger}$)**.** *Note that the matrix* $\mathcal{B}_u(1) = [B_{uh1}\ B_{uh2}]$ *is of full column rank according to their structures in* (10). *Thus,* L_1 *is a full-column matrix and its left inverse exists.*

Second, when the disturbance d is a two-dimensional signal that cannot be fully decoupled, the condition (16a) can no longer be satisfied. A common solution is to constrain the $\mathcal{H}_\infty$ norm of the transfer function from d to r to suppress the effect of d. Here, inspired by the approach in [19], we tackle the problem from a data-driven perspective. Specifically, we use the historical data of the disturbance to train the filter so that it is robust to the disturbance. To this end, let us split $H(\mathfrak{q},0)$ into two parts, i.e., $H(\mathfrak{q},0) = [E_1(\mathfrak{q},0)\ E_2]$, and matrices $E_1(\mathfrak{q},0), E_2$ are given by

$$E_1(\mathfrak{q},0) = \mathfrak{q}E_{11} + E_{10} = \begin{bmatrix} -\mathfrak{q}I + \mathcal{A}(0) \\ C \end{bmatrix},\ E_{11} = \begin{bmatrix} -I \\ 0 \end{bmatrix},\ E_{10} = \begin{bmatrix} \mathcal{A}(0) \\ C \end{bmatrix},\ E_2 = \begin{bmatrix} \mathcal{B}_d(0) \\ 0 \end{bmatrix},$$

where $E_1(\mathfrak{q},0)$ corresponds to the unknown internal state x that can be decoupled and E_2 corresponds to the non-decoupled disturbance d. We obtain

$$r = \frac{1}{a(\mathfrak{q})}N(\mathfrak{q})L_0[Y] = -\frac{1}{a(\mathfrak{q})}N(\mathfrak{q})H(\mathfrak{q},0)[X] = -\frac{1}{a(\mathfrak{q})}N(\mathfrak{q})E_1(\mathfrak{q},0)[x] - \frac{1}{a(\mathfrak{q})}N(\mathfrak{q})E_2[d]. \tag{17}$$

To make the residual as small as possible in the normal mode, we opt to decouple x from r, i.e.,

$$N(\mathfrak{q})E_1(\mathfrak{q},0)=0. \tag{18a}$$

We further suppose that the disturbance d comes from a prescribed probability space, and we have access to m independent identically distributed (i.i.d.) disturbance patterns d_i for $i\in\{1,\dots,m\}$. For each d_i, we define its contribution to the residual as

$$r_{d_i}=-\frac{1}{a(\mathfrak{q})}N(\mathfrak{q})E_2[d_i].$$

Therefore, we can mitigate the effects of the disturbance by constraining the $\mathcal{L}_2$ norm of r_{d_i} for all $i\in\{1,\dots,m\}$ in the normal mode, i.e.,

$$\frac{1}{m}\sum_{i=1}^{m}\|r_{d_i}\|_{\mathcal{L}_2}^2=\frac{1}{m}\sum_{i=1}^{m}\left\|\frac{1}{a(\mathfrak{q})}N(\mathfrak{q})E_2[d_i]\right\|_{\mathcal{L}_2}^2\le\beta, \tag{18b}$$

where $\beta\in\mathbb{R}_+$. We show later the approach to constructing $\|r_{d_i}\|_{\mathcal{L}_2}$ with a combination of the system model and the data d_i. The condition (16b) is adopted again to ensure the sensitivity of the residual to the faulty mode. Based on the above discussion, we formulate the second problem.

Problem 2. (Data-assisted robust fault detection filter design) *Consider the state-space model of the inverter-based microgrid system* (11) *with three-phase symmetrical ground faults and Assumption 2.1 with* $n_d=2$. *Given multiple instances of the disturbance* d_i *for* $i\in\{1,\dots,m\}$, *find a fault detection filter* $\mathbb{F}$ *in the form of* (13) *that satisfies the conditions* (18a), (18b), *and* (16b).

3. Main Results

In this section, we present two design methods of fault detection filters in two scenarios: one where the disturbance can be fully decoupled, and the other where it cannot be fully decoupled.

3.1. Filter design: perfect setting

We first consider the one-dimensional disturbance that can be fully decoupled. In order to find a feasible $N(\mathfrak{q})$ satisfying the conditions in Problem 1, we formulate the design of the fault detection filter as a LP problem in the following proposition.

Proposition 3.1 (Filter design: LP)**.** *Suppose that Assumption 2.1 holds and the dimension of the disturbance* $n_d=1$. *Consider the unified state-space model of the inverter-based microgrid system* (11), *and the structure of the fault detection filter in* (13). *Given the degree* d_N, *a stable* $a(\mathfrak{q})$, *and a scalar* $\gamma\in\mathbb{R}_+$, *the detection conditions* (16a) *and* (16b) *in Problem 1 are satisfied if*

$$\bar{N}\bar{H}(0)=0, \tag{18a}$$

$$\|\bar{N}\bar{L}\bar{H}(1)\|_\infty\ge\gamma, \tag{18b}$$

where $\bar{N}=[N_0,\ N_1,\ \dots,\ N_{d_N}]$, $\bar{L}=diag\underbrace{[L_0L_1^\dagger,\ \dots,\ L_0L_1^\dagger]}_{d_N+1}$,

$$\bar{H}(f)=\begin{bmatrix}H_0(f) & H_1 & 0 & \dots & 0\\ 0 & H_0(f) & H_1 & 0 & \vdots\\ \vdots & 0 & \ddots & \ddots & 0\\ 0 & \dots & 0 & H_0(f) & H_1\end{bmatrix},\ \text{and } f\in\{0,1\}.$$

Proof. According to the multiplication rule of polynomial matrices [19, Lemma 4.2], (16) can be written as

$$N(\mathfrak{q})H(\mathfrak{q},0) = \bar{N}\bar{H}(0)[I,\ \mathfrak{q}I,\ \ldots,\ \mathfrak{q}^{d_N+1}I]^\top, \tag{19a}$$

$$N(\mathfrak{q})L_0L_1^\dagger H(q,1) = \bar{N}\bar{L}\bar{H}(1)[I,\ \mathfrak{q}I,\ \ldots,\ \mathfrak{q}^{d_N+1}I]^\top. \tag{19b}$$

First, one can see from (19a) that $\bar{N}\bar{H}(0) = 0$ is equivalent to condition (16a), i.e., $N(\mathfrak{q})H(\mathfrak{q},0) = 0$. Therefore, the residual in the normal mode $r = N(\mathfrak{q})H(\mathfrak{q},0)[X] = 0$ and (16a) is satisfied. Second, we let the coefficients of $N(\mathfrak{q})L_0L_1^\dagger H(q,1)$ be nonzero through (18b). Thus, (16b) is satisfied, which ensures the fault sensitivity. This completes the proof. □

Note that $\bar{N}\bar{L}\bar{H}(1)$ is a row vector with $(d_N+2)(n_x+n_d)$ columns. For a positive scalar γ, $\|\bar{N}\bar{L}\bar{H}(1)\|_\infty \geq \gamma$ holds if and only if $\bar{N}\bar{L}\bar{H}(1)v_i \geq \gamma$ or $\bar{N}\bar{L}\bar{H}(1)v_i \leq -\gamma$, where v_i is a $(d_N+2)(n_x+n_d)$-dimensional column vector with only the i-th element be 1 and the rest are zero, i.e., $v_i = [0,\ldots,1,\ldots,0]^\top$. Moreover, it is easy to check that if $\bar{N}^*$ is a solution to (18), so is $-\bar{N}^*$. Therefore, one can replace the constraint (18b) with $\bar{N}\bar{L}\bar{H}(1)v_i$ (or $-\bar{N}\bar{L}\bar{H}(1)v_i$) and view (18) as a set of $(d_N+2)(n_x+n_d)$ LP problems.

Remark 3.2 (Feasibility analysis)**.** *According to the well-known rank plus nullity theorem, we have* $(d_N+1)(n_x+n_y) = \mathrm{Rank}(\bar{H}(0)) + \mathrm{Null}(\bar{H}(0))$*, where* $\mathrm{Rank}(\bar{H}(0))$ *and* $\mathrm{Null}(\bar{H}(0))$ *denote the rank and the left null space dimension of* $\bar{H}(0)$*, respectively. Thus, the constraint* (18) *is feasible when* $\mathrm{Null}(\bar{H}(0)) \neq 0$*, i.e.,* $(d_N+1)(n_x+n_y) > \mathrm{Rank}(\bar{H}(0))$*. For the constraint* $\|\bar{N}\bar{L}\bar{H}(1)\|_\infty \geq \gamma$*, it is required that* $\bar{L}\bar{H}(1)$ *does not belong to the column range space of* $\bar{H}(0)$*, i.e.,* $\mathrm{Rank}([\bar{H}(0)\ \bar{L}\bar{H}(1)]) > \mathrm{Rank}(\bar{L}\bar{H}(1))$*. Otherwise, a feasible* $\bar{N}$ *to* (18a) *leads to* $\bar{N}\bar{L}\bar{H}(1) = 0$*.*

3.2. **Filter design: non-decoupled disturbance**

In this subsection, we consider the disturbance d that cannot be fully decoupled. Recall that the residual r in the normal mode depends on the internal state x and the disturbance d from the right-hand side of (17). For one instance of disturbances $d_i = [d_i(1),\ldots,d_i(T)]$ with a time horizon $T \in \mathbb{N}$, recall that its contribution to the residual is $r_{d_i} = -a^{-1}(\mathfrak{q})N(\mathfrak{q})E_2[d_i]$. Then, the response of the j-th element of d_i, i.e., $d_i(j)$, can be computed by

$$\left[r_{d_i(j)}(1),\ r_{d_i(j)}(2),\ \ldots,\ r_{d_i(j)}(T)\right] = -N(\mathfrak{q})E_2 d_i(j)\ell_j,$$

where $\ell_j = [\overbrace{0,\ldots,0}^{j-1},\bar{\ell}(1),\bar{\ell}(2),\ldots,\bar{\ell}(T-j+1)]$ and $\bar{\ell}(k)$ for $k \in \mathbb{N}$ is the value of the discrete-time unit impulse response of $a^{-1}(\mathfrak{q})$ at time instance k. By summing up the response of $d_i(j)$ for $j \in \{1,\ldots,T-d_N-1\}$, we obtain

$$\begin{aligned}[r_{d_i}(1),\ r_{d_i}(2),\ \ldots,\ r_{d_i}(T)] &= -N(\mathfrak{q})E_2 \sum_{j=1}^{T-d_N-1} d_i(j)\ell_j \\ &= -\bar{N}\bar{E}_2 \begin{bmatrix} I \\ \mathfrak{q}I \\ \vdots \\ \mathfrak{q}^{d_N+1} \end{bmatrix} [d_i(1),\ \ldots,\ d_i(T-d_N-1)] \begin{bmatrix} \ell_1 \\ \vdots \\ \ell_{T-d_N-1} \end{bmatrix}, \end{aligned} \tag{20}$$

where $\bar{E}_2 = \mathrm{diag}(E_2, \dots, E_2)$ according to the multiplication rule of polynomial matrices. Recall that $\mathfrak{q}$ is a time shift operator, i.e., $\mathfrak{q} d_i(k) = d_i(k+1)$. Thus, the equation (20) can be written as

$$\begin{aligned}[r_{d_i}(1),\ r_{d_i}(2),\ \dots,\ r_{d_i}(T)] &= -\bar{N}\bar{E}_2 \begin{bmatrix} d_i(1) & \dots & d_i(T-d_N-1) \\ d_i(2) & \dots & d_i(T-d_N) \\ \vdots & \ddots & \vdots \\ d_i(d_N+2) & \dots & d_i(T) \end{bmatrix} \begin{bmatrix} \ell_1 \\ \vdots \\ \ell_{T-d_N-1} \end{bmatrix} \\ &= -\bar{N}\bar{E}_2 D_i \Gamma. \end{aligned} \tag{21}$$

To ensure the existence of D_i, we assume that the length of data T is greatly larger than $d_N + 1$, i.e., $T \gg d_N + 1$. With (21), the $\mathcal{L}_2$ norm of r_{d_i} as considered in Problem 2 is formulated into the quadratic form

$$\|r_{d_i}\|_{\mathcal{L}_2}^2 = \bar{N}\Phi_i\bar{N}^\top, \quad \Phi_i = \bar{E}_2 D_i \Gamma (\bar{E}_2 D_i \Gamma)^\top. \tag{22}$$

It is worth emphasizing that Φ_i is positive semi-definite since $\|r_{d_i}\|_{\mathcal{L}_2}^2 = \bar{N}\Phi_i\bar{N}^\top \geq 0$ for all non-zero $\bar{N}$.

Now, we can present the design method of the fault detection filter in the presence of the non-decoupled disturbance in the following theorem.

Theorem 3.3 (Filter design: QP)**.** *Consider the unified state-space model of the inverter-based microgrid system* (11)*, Assumption 2.1 with the two-dimensional disturbance, and the structure of the fault detection filter in* (13)*. Given the degree d_N, a stable $a(\mathfrak{q})$ and multiple instances of disturbance $d_i = [d_i(1), \dots, d_i(T)]$ for $i \in \{1, \dots, m\}$ with $T \gg d_N$, conditions* (18a)*,* (18b)*,* (16b) *in Problem 2 are satisfied by solving the following optimization problem*

$$\min_{\bar{N}} \ \bar{N}\bar{\Phi}\bar{N}^\top - \|\bar{N}\bar{L}\bar{H}(1)\|_\infty \quad \text{s.t. } \bar{N}\bar{E}_1 = 0, \tag{23}$$

where $\bar{\Phi} = \frac{1}{m}\sum_{i=1}^m \Phi_i$,

$$\bar{E}_1 = \begin{bmatrix} E_{10} & E_{11} & 0 & \dots & 0 \\ 0 & E_{10} & E_{11} & 0 & \vdots \\ \vdots & 0 & \ddots & \ddots & 0 \\ 0 & \dots & 0 & E_{10} & E_{11} \end{bmatrix}.$$

Proof. The first term in the objective function, i.e., $\bar{N}\bar{\Phi}\bar{N}^\top$, relates to the condition (18b), which ensures that the effects of different instances of disturbances on the residual are bounded. We show the derivation process of the quadratic form of $\|r_{d_i}\|_{\mathcal{L}_2}^2$ in (20)-(22). The second term in the objective function, i.e., $-\|\bar{N}\bar{L}\bar{H}(1)\|_\infty$, relates to the condition (16b), which is introduced to ensure the sensitivity of the residual to the faulty mode. The constraint $\bar{N}\bar{E}_1 = 0$ related to the condition (18a) is used to decouple the internal state x from the residual. One can show through the multiplication rule of polynomial matrices that $N(\mathfrak{q})E_1(\mathfrak{q}, 0) = 0 \Leftrightarrow \bar{N}\bar{E}_1 = 0$. This completes the proof. □

Note that the optimization problem (23) can be viewed as a set of $(d_N+2)(n_x+n_d)$ QP problems by replacing $\|\bar{N}\bar{L}\bar{H}(1)\|_\infty$ with $\bar{N}\bar{L}\bar{H}(1)v_i$ (or $-\bar{N}\bar{L}\bar{H}(1)v_i$) as analyzed before. Recall that $v_i = [0, \dots, 1, \dots, 0]^\top$. In addition, the matrix Φ_i is positive semi-definite, and thus the derived QP problems are convex and tractable. We further propose an approximate analytical solution to (23) in the following corollary.

Corollary 3.4 (Approximate analytical solution)**.** *Consider the optimization problem* (23)*. There exists an approximate analytical solution given by the following form:*

$$\bar{N}^*(\delta) = \frac{1}{2\delta}\left(\bar{L}\bar{H}(1)v_i^*\right)^\top \left(\delta^{-1}\bar{\Phi} + \bar{E}_1\bar{E}_1^\top\right)^{-1}, \tag{24}$$

where $v_i^* = \arg\max_{i\in\{1,\ldots,(d_N+2)(n_x+n_d)\}} |\bar{N}^*(\delta)\bar{L}\bar{H}(1)v_i|$ *and* $\delta \in \mathbb{R}_+$ *is the Lagrange multiplier. The solution* $\bar{N}^*(\delta)$ *provides an approximate solution to* (23) *and will converge to the optimal solution as* δ *tends to* ∞*.*

Proof. The proof is similar to that of [22, Corollary 3.4] and thus is omitted here. □

Remark 3.5 (Average objective function)**.** *To ensure that the derived fault detection filter is robust to the disturbance, we consider* m *different disturbance patterns* d_i *for* $i \in \{1,\ldots,m\}$ *and take the average effects of all* d_i *on the residual as the objective function in* (23)*. An alternative way is to consider the worst-case scenario as the objective function, i.e.,* $\max_{i\in\{1,\ldots,m\}} \bar{N}\Phi_i\bar{N}^\top$*. The average objective function is, however, of interest if one requires to train the filter with a large number of disturbance patterns. This is due to the fact that the computational complexity of the derived QP problem is independent of the number of disturbance patterns* m *with the average objective function.*

Remark 3.6 (Online updating of coefficients)**.** *In [19], the authors construct the objective function using the nonlinearity signature to ensure that the derived filter is robust to the nonlinear terms. Compared to [19], we further derive an approximate analytical solution to the optimization problem* (23)*. With the analytical solution, one can update the coefficients of the filter online with new data without the need to re-solve* (23)*. This is a significant improvement over [19].*

Remark 3.7 (Approximate analytical solution with δ)**.** *The Lagrange multiplier* δ *is introduced in* (23) *to penalize the equality constraint* $\bar{N}\bar{E}_1 = 0$*, and in the ideal case,* δ *tends to infinity as stated in Corollary 3.4. However, for a bounded* δ*, the equality constraint cannot be strictly satisfied, which is why we refer to the solution* (24) *as an approximate analytical solution. Additionally, to ensure that* $\bar{N}\bar{E}_1$ *is sufficiently close to zero,* δ *should be large enough while remaining numerically bounded for practical considerations.*

To detect the fault, we introduce the power of the residual $r(k)$ as the evaluation function, i.e., $J(r) = r(k)^2$ for $k \in \mathbb{N}$. Let J_{th} be the detection threshold. Then, we can consider the following detection logic:

$$\begin{cases} J(r) \le J_{th} & \Rightarrow \quad \text{no faults,} \\ J(r) > J_{th} & \Rightarrow \quad \text{faults.} \end{cases}$$

It is worth emphasizing that false alarms are inevitable due to the random nature of the residual. We show the computation method of the threshold and the false alarm rate in the following proposition.

Proposition 3.8 (Probabilistic false alarm certificate)**.** *Assume that the disturbance patterns follow the i.i.d. distribution. Consider the system* (11)*, the filter* $\mathbb{F}(\mathfrak{q})$ *obtained by using* (23) *with the corresponding solution* $\bar{N}^*$*, and the evaluation function* $J(r) = r(k)^2$ *for* $k \in \mathbb{N}$*. Given a scalar* $\lambda \ge 1$*, if we set the threshold* J_{th} *as*

$$J_{th} = \frac{\lambda}{T}\bar{N}^*\bar{\Phi}\bar{N}^{*\top}, \tag{25}$$

the false alarm rate in the steady state satisfies

$$\lim_{k\to\infty} \mathbf{Pr}\{J(r(k)) > J_{th} | f = 0\} = \lim_{T,k,m\to\infty} \mathbf{Pr}\left\{ r(k)^2 > \frac{\lambda}{T}\bar{N}^* \left(\frac{1}{m}\sum_{i=1}^{m}\Phi_i\right)\bar{N}^{*\top} \Big| f = 0 \right\} \leq \frac{1}{\lambda}. \quad (26)$$

Proof. Since the disturbance d comes from a prescribed probability space and each disturbance pattern follows i.i.d. distribution, the residual in the health mode, i.e., $r = -a^{-1}(\mathfrak{q})N(\mathfrak{q})E_2[d]$, can be viewed as a random variable on the same probability space as d. It is proven in [19, Theorem 4.11] that the empirical average error

$$e_m = \frac{1}{m}\sum_{i=1}^{m} \|r_{d_i}\|_{\mathcal{L}_2}^2 - \mathbf{E}\left[\|r\|_{\mathcal{L}_2}^2\right],$$

satisfies the strong law of large numbers, i.e., $\lim_{m\to\infty} e_m = 0$ almost surely. Therefore, it holds that

$$\lim_{T,m\to\infty} \frac{\lambda}{T}\bar{N}^* \left(\frac{1}{m}\sum_{i=1}^{m}\Phi_i\right)\bar{N}^{*\top} = \lim_{T,m\to\infty} \frac{\lambda}{T}\frac{1}{m}\sum_{i=1}^{m}\|r_{d_i}\|_{\mathcal{L}_2}^2 = \lim_{T\to\infty}\frac{\lambda}{T}\mathbf{E}\left[\|r\|_{\mathcal{L}_2}^2\right] = \lambda \lim_{k\to\infty}\mathbf{E}[r(k)^2].$$

According to Markov inequality, the false alarm rate in the steady state satisfies

$$\lim_{k\to\infty} \mathbf{Pr}\{r(k)^2 > \lambda \mathbf{E}[r(k)^2] | f = 0\} \leq \frac{1}{\lambda}.$$

This completes the proof. □

4. Simulation results

In this section, we validate the performance of the fault detection filters through numerical simulations. The optimization problems are solved through the YALMIP toolbox [28]. Consider the inverter-based microgrid system depicted in Figure 1. We refer to the parameters and initial conditions in [23], which are presented in Table 1 and Table 2, respectively. The reference voltage (operating point) of the microgrid is $v_{odq}^* = [381, 0]^\top$ and the FCL parameter is $\tau_{dq} = [35, 0.7]^\top$, which are assumed to be constant during the experiment. The sampling period is 0.1 ms and the simulation time is 500 ms.

Table 1. Microgrid parameters.

Parameter	Value	Parameter	Value
f	50 Hz	R_{LOAD}	12 Ω
L_f	0.1 mH	K_P^c	28
R_f	0.1 Ω	K_I^c	5
C_f	30μ F	K_P^v	0.1
L_c	1 mH	K_I^v	170
R_c	0.03 Ω	F	0.75
ω	314.1		

Table 2. Initial conditions.

Parameter	Value	Parameter	Value
v_{od}	380.8	i_{ld}	11.4
v_{oq}	0	i_{lq}	-5.5×10^3
i_{od}	11.4	v_{bd}	379.5
i_{oq}	0.4	v_{bq}	-6
ϕ_d	0.13	γ_d	0.0115
ϕ_q	0	γ_q	0

4.1. Scenario 1: Perfect setting

We first consider the perfect setting with one-dimensional disturbances that can be fully decoupled, as described in Remark 2.2. We set the matrix $B_d = \begin{bmatrix}\mathbf{0}_{1\times 8} & [1\ 1]\end{bmatrix}^\top$. The disturbance is zero for $k \leq 1000$, and subsequently follows a signal given by $d(k) = \alpha_0 + \sum_{i=1}^{\eta}\alpha_i \sin(\omega_i k + \psi_i)$ for $k > 1000$. Specifically, the constant $\alpha_0 \in \mathbb{R}$ represents an abrupt change, while the sinusoidal terms capture the short-term load fluctuations with amplitudes α_i, angular frequencies $\omega_i \in \mathbb{R}_+$,

and phases $\psi_i \in \mathbb{R}$ [19]. It is worth emphasizing that we deliberately select the parameters of B_d and magnitude of d to make the output currents similar in the faulty mode and under the effect of the disturbance, which increases the difficulty of fault detection.

To design the fault detection filter in the form of (13), we fix the degree of $N(\mathfrak{q})$ to be $d_N = 10$, set $\gamma = 0.5$, and choose a stable denominator $a(\mathfrak{q})$ with a degree larger than d_N. We then apply Proposition 3.1 to construct the fault detection filter for inverter-based microgrid systems with the disturbance that can be fully decoupled. The detection threshold is set to $J_{th} = 1 \times 10^{-5}$. The simulation results are presented in Figure 2.

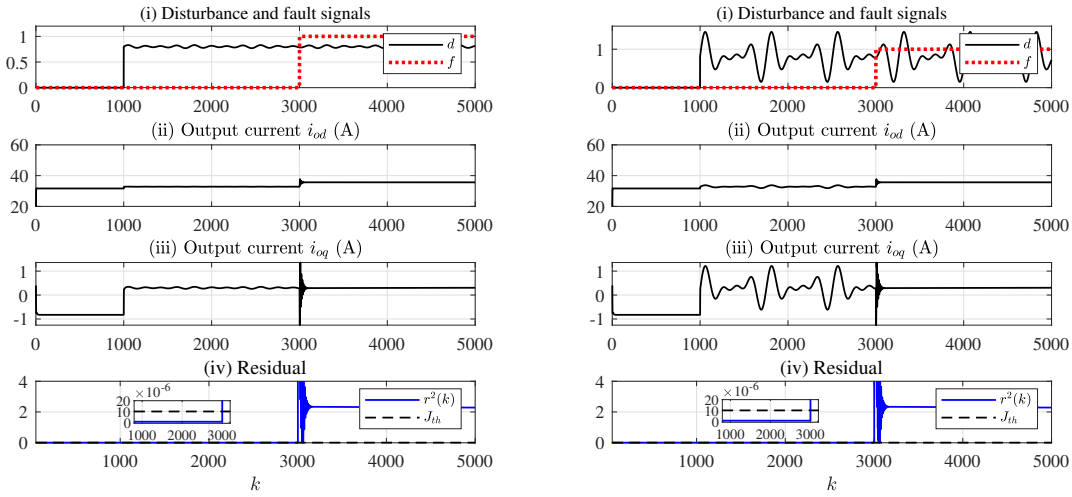

(a) Small load fluctuations.

(b) Large load fluctuations.

FIGURE 2. Diagnosis results by using (18) with decoupled disturbances.

Figure 2a presents the diagnosis results when a decoupled disturbance has small load fluctuations, i.e., $d(k) = 0.8 + 0.02\sin(k/30) + 0.01\sin(k/40) + 0.01\sin(k/60)$. As shown in Figure 2a (i), the disturbance d and the ground fault f occur at $k = 1001$ and $k = 3001$, respectively. However, d and f have similar effects on the output currents i_{od} and i_{oq} from Figure 2a (ii) and (iii), which only exhibit minor variations. This makes it challenging to detect the occurrence of the ground fault and distinguish it from the disturbance only through the output currents. In contrast, Figure 2a (iv) illustrates that the residual is insensitive to the disturbance and stays below the threshold until the fault happens. The power value of the residual $r^2(k)$ exceeds the threshold at $k = 3002$, resulting in the detection of the fault within 0.1 ms. We further consider a decoupled disturbance with larger load fluctuations, i.e., $d(k) = 0.8 + 0.2\sin(k/30) + 0.3\sin(k/40) + 0.2\sin(k/60)$. Figure 2b displays the diagnosis results and the analysis process is analogous to the previous one.

4.2. **Scenario 2: Non-decoupled disturbance**

In this subsection, we consider two-dimensional disturbances that cannot be fully decoupled. The matrix $B_d = \begin{bmatrix}\mathbf{0}_{2\times 8} & \text{diag}([0.5\ 0.5])\end{bmatrix}^\top$ here. To capture the disturbance, we denote the space of disturbance patterns by

$$d(k) = \begin{bmatrix}\alpha_{d,0} + \sum_{i=1}^{\eta} \alpha_{d,i}\sin(\omega_{d,i}k + \psi_{d,i}) \\ \alpha_{q,0} + \sum_{i=1}^{\eta} \alpha_{q,i}\sin(\omega_{q,i}k + \psi_{q,i})\end{bmatrix},$$

where the parameters $(\alpha_{d,i})_{i=0}^{\eta}$, $(\alpha_{q,i})_{i=0}^{\eta}$, $(\omega_{d,i})_{i=1}^{\eta}$, $(\omega_{q,i})_{i=1}^{\eta}$, $(\psi_{d,i})_{i=1}^{\eta}$, $(\psi_{q,i})_{i=1}^{\eta}$, and η are random variables and follow uniform distributions in certain bounds. We generate 30 disturbance patterns (i.e., $m = 30$ in (18b)) and choose the time horizon $T = 50$. Again, we fix $d_N = 10$ and choose a stable denominator $a(\mathfrak{q})$. With the above settings, we can generate the matrix $\bar{\Phi}$ in the objective function of the optimization problem (23). We construct robust fault detection filters by using Theorem 3.3 to deal with the fault detection problem for inverter-based microgrid systems with non-decoupled disturbances. The simulation results are presented in Figure 3.

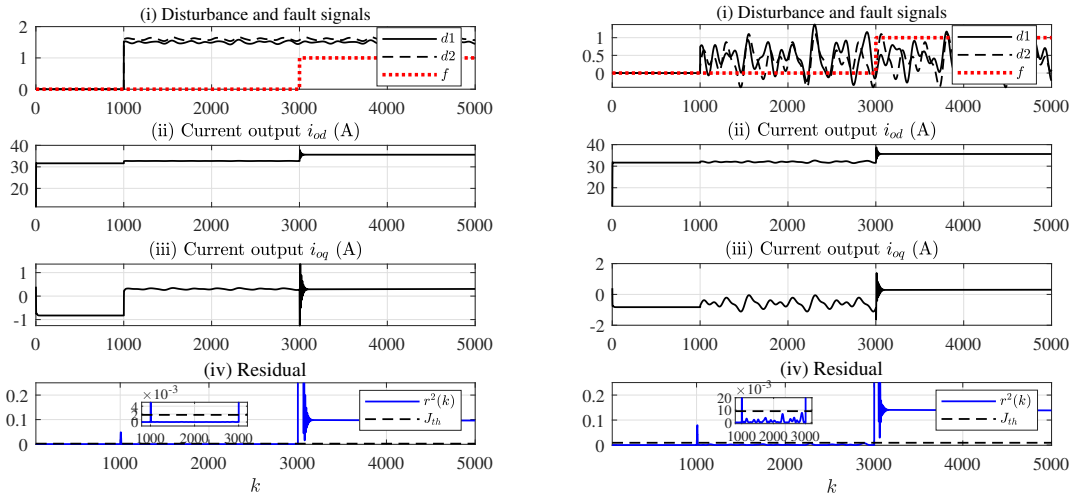

(a) Small load fluctuations.

(b) Large load fluctuations.

FIGURE 3. Diagnosis results by using (18) with decoupled disturbances.

Figure 3a provides the diagnosis result by using (23) in the presence of a non-decoupled disturbance with small load fluctuations. Let $U(l_1, l_2)$ denote a uniform distribution taking values between l_1 and l_2. Then, for disturbances with small load fluctuations, the parameters of the disturbance d are $\alpha_{d,0}, \alpha_{q,0} \sim U[1, 2]$, $\alpha_{d,i}, \alpha_{q,i} \sim U[0, 0.05]$, $\omega_{d,i}, \omega_{q,i} \sim U[1/80, 1/40]$, and $\psi_{d,i}, \psi_{q,i} \sim U[0, 100]$. We compute the threshold $J_{th} = 0.0018$ based on (25) with $\lambda = 3$. As shown in Figure 3a (i), the disturbance d and the ground fault f happen at $k = 1001$ and $k = 3001$, respectively. However, it is difficult to distinguish d and f through the output currents from Figure 3a (ii) and (iii). The power value of the residual $r^2(k)$ is shown in Figure 3a (iv), one can see that $r^2(k)$ remains below the threshold in the presence of non-decoupled disturbances until the occurrence of the fault at $k = 3001$. This suggests that the proposed filter effectively suppresses the effects of disturbances on the residual. Although there is a spike in the residual caused by the transient response of the step signal in disturbances, it disappears quickly. However, after the fault happens, the value of $r^2(k)$ immediately exceeds the threshold and remains significantly higher than zero. This indicates that the fault is successfully detected and is distinguishable from the disturbance through the residual. To further verify the robustness of the fault detection filter to disturbances, we opted for a non-decoupled disturbance with larger fluctuations, where $\alpha_{d,0}, \alpha_{q,0} \sim U[0.5, 1]$, $\alpha_{d,i}, \alpha_{q,i} \sim U[0, 0.5]$, $\omega_{d,i}.\omega_{q,i} \sim U[1/60, 1/30]$, and $\psi_{d,i}, \psi_{q,i} \sim U[0, 100]$. Since the disturbance patterns vary, it is necessary to regenerate the matrix $\bar{\Phi}$ and design the filter using (23). We calculated the threshold

$J_{th} = 0.0091$ based on (25) with $\lambda = 10$. The diagnosis results in the presence of large load fluctuations are presented in Figure 3b. The analysis process is similar to the previous one and, therefore, omitted here.

5. Conclusions

In this paper, we propose diagnosis strategies for the detection of ground faults in inverter-based microgrid systems with decoupled and non-decoupled disturbances, respectively. Our strategies involve developing fault detection filters to deal with disturbances and ensure fault sensitivity. To achieve this, we reformulate the filter design problem into tractable optimization problems, which enable us to efficiently optimize the filter parameters and meet the desired performance criteria. Simulation results on an inverter-based microgrid system that works in the islanded mode show the effectiveness of the proposed approaches. In future work, we first will consider designing the denominator of the filter for better dynamic performance. The second direction will be focused on extending the proposed approaches to more complex and realistic settings, such as considering the presence of multiple converters that introduce nonlinearity into the model.

Acknowledgement

The authors are grateful to M. Popov and A. Lekic for the valuable discussion on inverter-based microgrid systems.

References

[1] M. W. Altaf, M. T. Arif, S. N. Islam, M. E. Haque, Microgrid protection challenges and mitigation approaches-a comprehensive review, IEEE Access (2022).

[2] M. A. Zamani, A. Yazdani, T. S. Sidhu, A communication-assisted protection strategy for inverter-based medium-voltage microgrids, IEEE Transactions on Smart Grid 3 (4) (2012) 2088–2099.

[3] K. Lai, M. S. Illindala, M. A. Haj-ahmed, Comprehensive protection strategy for an islanded microgrid using intelligent relays, in: 2015 IEEE Industry Applications Society Annual Meeting, IEEE, 2015, pp. 1–11.

[4] H. Karimi, G. Shahgholian, B. Fani, I. Sadeghkhani, M. Moazzami, A protection strategy for inverter-interfaced islanded microgrids with looped configuration, Electrical Engineering 101 (3) (2019) 1059–1073.

[5] D. G. Photovoltaics, E. Storage, IEEE application guide for IEEE std 1547™, IEEE standard for interconnecting distributed resources with electric power systems, IEEE std (2009) 1547–2.

[6] T. Loix, T. Wijnhoven, G. Deconinck, Protection of microgrids with a high penetration of inverter-coupled energy sources, in: 2009 CIGRE/IEEE PES Joint Symposium Integration of Wide-Scale Renewable Resources Into the Power Delivery System, IEEE, 2009, pp. 1–6.

[7] E. Casagrande, W. L. Woon, H. H. Zeineldin, D. Svetinovic, A differential sequence component protection scheme for microgrids with inverter-based distributed generators, IEEE Transactions on Smart Grid 5 (1) (2013) 29–37.

[8] S. Samantaray, G. Joos, I. Kamwa, Differential energy based microgrid protection against fault conditions, in: 2012 IEEE PES Innovative Smart Grid Technologies (ISGT), IEEE, 2012, pp. 1–7.

[9] E. Sortomme, S. Venkata, J. Mitra, Microgrid protection using communication-assisted digital relays, IEEE Transactions on Power Delivery 25 (4) (2009) 2789–2796.

[10] X. Li, A. Dyśko, G. M. Burt, Traveling wave-based protection scheme for inverter-dominated microgrid using mathematical morphology, IEEE Transactions on Smart Grid 5 (5) (2014) 2211–2218.

[11] L. Liu, Z. Liu, M. Popov, P. Palensky, M. A. van der Meijden, A fast protection of multi-terminal hvdc system based on transient signal detection, IEEE Transactions on Power Delivery 36 (1) (2020) 43–51.

[12] H. Karimi, A. Yazdani, R. Iravani, Negative-sequence current injection for fast islanding detection of a distributed resource unit, IEEE Transactions on Power Electronics 23 (1) (2008) 298–307.

[13] M. Pirani, M. Hosseinzadeh, J. A. Taylor, B. Sinopoli, Optimal active fault detection in inverter-based grids, IEEE Transactions on Control Systems Technology (2022).

[14] Z. Gao, C. Cecati, S. X. Ding, A survey of fault diagnosis and fault-tolerant techniques—part I: Fault diagnosis with model-based and signal-based approaches, IEEE Transactions on Industrial Electronics 62 (6) (2015) 3757–3767.

[15] R. J. Patton, J. Chen, On eigenstructure assignment for robust fault diagnosis, International Journal of Robust and Nonlinear Control: IFAC-Affiliated Journal 10 (14) (2000) 1193–1208.

[16] Z. Gao, X. Liu, M. Z. Chen, Unknown input observer-based robust fault estimation for systems corrupted by partially decoupled disturbances, IEEE Transactions on Industrial Electronics 63 (4) (2015) 2537–2547.

[17] J. Chen, R. J. Patton, H.-Y. Zhang, Design of unknown input observers and robust fault detection filters, International Journal of Control 63 (1) (1996) 85–105.

[18] M. Nyberg, E. Frisk, Residual generation for fault diagnosis of systems described by linear differential-algebraic equations, IEEE Transactions on Automatic Control 51 (12) (2006) 1995–2000.

[19] P. Mohajerin Esfahani, J. Lygeros, A tractable fault detection and isolation approach for nonlinear systems with probabilistic performance, IEEE Transactions on Automatic Control 61 (3) (2015) 633–647.

[20] K. Pan, P. Palensky, P. Mohajerin Esfahani, Dynamic anomaly detection with high-fidelity simulators: A convex optimization approach, IEEE Transactions on Smart Grid 13 (2) (2021) 1500–1515.

[21] C. Van der Ploeg, M. Alirezaei, N. Van De Wouw, P. Mohajerin Esfahani, Multiple faults estimation in dynamical systems: Tractable design and performance bounds, IEEE Transactions on Automatic Control 67 (9) (2022) 4916–4923.

[22] C. van der Ploeg, E. Silvas, N. van de Wouw, P. Mohajerin Esfahani, Real-time fault estimation for a class of discrete-time linear parameter-varying systems, IEEE Control Systems Letters 6 (2021) 1988–1993.

[23] N. Pogaku, M. Prodanovic, T. C. Green, Modeling, analysis and testing of autonomous operation of an inverter-based microgrid, IEEE Transactions on Power Electronics 22 (2) (2007) 613–625.

[24] S. Leitner, M. Yazdanian, A. Mehrizi-Sani, A. Muetze, Small-signal stability analysis of an inverter-based microgrid with internal model-based controllers, IEEE Transactions on Smart Grid 9 (5) (2017) 5393–5402.

[25] R. H. Park, Two-reaction theory of synchronous machines generalized method of analysis-part I, Transactions of the American Institute of Electrical Engineers 48 (3) (1929) 716–727.

[26] Y. Xu, Robust finite-time control for autonomous operation of an inverter-based microgrid, IEEE Transactions on Industrial Informatics 13 (5) (2017) 2717–2725.

[27] S. X. Ding, Model-based fault diagnosis techniques: design schemes, algorithms, and tools, Springer Science & Business Media, 2008.

[28] J. Löfberg, Yalmip : A toolbox for modeling and optimization in matlab, in: In Proceedings of the CACSD Conference, Taipei, Taiwan, 2004.